applied sciences

MDPI

Article

Signal Acquisition and Algorithm Design for Bioimpedance-Based Heart Rate Estimation from the Wrist

Didzis Lapsa [1,2,*], Margus Metshein [3,*], Andrei Krivošei [3], Rims Janeliukstis [1], Olev Märtens [3] and Atis Elsts [1]

[1] Institute of Electronics and Computer Science, Dzerbenes Street 14, LV-1006 Riga, Latvia; rimasj479@gmail.com (R.J.); atis.elsts@edi.lv (A.E.)
[2] Faculty of Computing, University of Latvia, Raiņa Bulvāris 19, LV-1586 Riga, Latvia
[3] Thomas Johann Seebeck Department of Electronics, Tallinn University of Technology, Ehitajate tee 5, 19086 Tallinn, Estonia; andrei.krivosei@taltech.ee (A.K.); olev.martens@taltech.ee (O.M.)
* Correspondence: didzis.lapsa@edi.lv (D.L.); margus.metshein@taltech.ee (M.M.)

Abstract: Background: Heart rate (HR) is a critical biomarker that provides insights into overall health, stress levels, and the autonomic nervous system. Pulse wave signals contain valuable information about the cardiovascular system and heart status. However, signal acquisition in wearables poses challenges, particularly when using electrical sensors, due to factors like the distance from the heart, body movement, and suboptimal electrode placement. Methods: Electrical bioimpedance (EBI) measurements using bipolar and tetrapolar electrode systems were employed for pulse wave signal acquisition from the wrist in both perpendicular and distal configurations. Signal preprocessing techniques, including baseline removal via Hankel matrix methods, normalization, cross-correlation, and peak detection, were applied to improve signal quality. This study describes the combination of sensor-level signal acquisition and processing for accurate wearable HR estimation. Results: The bipolar system was shown to produce larger $\Delta Z(t)$, while the tetrapolar system demonstrated higher sensitivity. Distal placement of the electrodes yielded greater $\Delta Z(t)$ (up to 0.231 Ω) when targeting both wrist arteries. Bandpass filtering resulted in a better signal-to-noise ratio (SNR), achieving 3.6 dB for the best bipolar setup and 4.8 dB for the tetrapolar setup, compared to 2.6 and 3.3 dB SNR, respectively, with the Savitzky–Golay filter. The custom HR estimation algorithm presented in this paper demonstrated improved accuracy over a reference method, achieving an average error of 1.8 beats per minute for the best bipolar setup, with a mean absolute percentage error (MAPE) of 8%. Conclusions: The analysis supports the feasibility of using bipolar electrode setups on the wrist and highlights the importance of electrode positioning relative to the arteries. The proposed signal processing method, featuring a preprocessing pipeline and HR estimation algorithm, provides a proof-of-concept demonstration for HR estimation from EBI signals acquired at the wrist.

Keywords: bipolar electrode system; electrical bioimpedance; heart rate estimation; peak detection; signal-to-noise ratio; tetrapolar electrode system

check for updates

Citation: Lapsa, D.; Metshein, M.; Krivošei, A.; Janeliukstis, R.; Märtens, O.; Elsts, A. Signal Acquisition and Algorithm Design for Bioimpedance-Based Heart Rate Estimation from the Wrist. *Appl. Sci.* **2024**, *14*, 9632. https://doi.org/10.3390/app14219632

Academic Editors: Roger Narayan, Luigi Bibbò and Alessia Bramanti

Received: 11 August 2024
Revised: 1 October 2024
Accepted: 16 October 2024
Published: 22 October 2024

Copyright: © 2024 by the authors. Licensee MDPI, Basel, Switzerland. This article is an open access article distributed under the terms and conditions of the Creative Commons Attribution (CC BY) license (https://creativecommons.org/licenses/by/4.0/).

1. Introduction

Heart rate (HR) is one of the four vital signs, serving as a key indicator of human psychophysiological condition. For example, heart rate variability (HRV) provides insights into the functionality of the autonomic nervous system [1]. An overview of the physiological basis of both HR and HRV can be found in [2]. Resting heart rate (HR) typically ranges between 60 and 100 beats per minute (BPM). The primary types of arrhythmias are classified as bradycardia (<60 BPM), tachycardia (>100 BPM), fibrillation, and premature contraction [3]. Therefore, accurate HR and cardiovascular parameter estimation are critical tasks in medical and personal healthcare practices (see an excellent review in [4]).

Electrical bioimpedance (EBI), which estimates the electrical properties of biological tissues, is a promising tool for noninvasive and unobtrusive cardiovascular parameter

acquisition [5]. The volume changes in arterial blood flow appear in the measured EBI signal as amplitude modulation, reflecting hemodynamic parameters including cardiovascular condition and heart functionality [6]. A well-known application of EBI is impedance cardiography (ICG) [7], which relies on the first derivative of the thoracic EBI signal. ICG can output timely changes in impedance, from which numerous cardiodynamic parameters can be estimated, such as stroke volume and cardiac output [6]. Recent studies have also shown that ICG can be extracted from the arm and wrist [8,9].

The importance of the HR acquisition site has been emphasized in the literature (e.g., in [10]) For instance, the thorax is a classical site for heart-related signal acquisition, as seen in ICG [7]. Another traditional method involves detecting HR-related volume changes between two limbs (such as the legs [11]). While the wrist is a convenient location for wearing a device, being a common site for a wristwatch, the cardiac volume change-related modulation in the measured signal is shallower and more prone to motion artifacts, which necessitates more intensive signal processing.

EBI-based measurement systems, particularly those designed for autonomous wearable use on the wrist, are relatively new. As a result, there is no widely accepted standard HR estimation algorithm specifically tailored for this method. While established HR estimation algorithms exist for photoplethysmography (PPG) and electrocardiography (ECG) [12], due to the fundamental differences in signal acquisition, these algorithms cannot be directly applied to EBI signals. Tailored algorithms, like the one presented in this paper, are needed to optimize HR estimation in EBI systems and address the unique challenges posed by this modality.

At the same time, EBI-based HR estimation offers several advantages over traditional methods such as PPG and ECG, particularly in wearable applications. They include:

- Increased resistance to measurement errors caused by varying skin tones, which can affect the accuracy of PPG systems. EBI measurements are based on the electrical properties of tissues, making the signal consistent across all skin types [13].
- Ability to measurement additional physiological parameters such as breathing, hydration, and sweating. This added capability makes EBI a more versatile tool for comprehensive health monitoring.

The two basic electrode systems for EBI measurement are bipolar (1) and tetrapolar (2) [6]. In the first case, a single pair of electrodes is used for both excitation and measurement [6,14]. In the second case, separate pairs of electrodes are used for these tasks. When using the bipolar system, the electrode impedances, lead wires, and contact interface are measured as a sum of the impedance values in the object [6]. The applicability of the bipolar system for forearm EBI measurements has been reported in the literature before [15–17]. However, these studies were either limited to simulation models [15], small trials with a single configuration [16], or focused on the electrode's physical properties without attention to the exact configuration and setup on the wrist surface [17].

The tetrapolar system has traditionally been used for measuring small impedance changes [18], such as in pulse wave detection [13]. Bipolar systems are typically used for body composition analysis [19] or to detect slow physiological processes, such as wound healing [20] or dehydration [21]. The potential applicability of the bipolar system for EBI-based pulse wave monitoring has been highlighted in [16], noting only a slightly lower signal-to-noise ratio (SNR) compared to other methods. Various SNR evaluation approaches have been described in the literature (e.g., [22]). The SNR evaluation method applied in this research is thoroughly described in [17,23].

EBI measurements are highly susceptible to motion artifacts, particularly in bipolar systems, as these artifacts stem from the skin-electrode interface and tissue movements like muscle contractions [24,25]. Estimating hemodynamic parameters during daily activities is complex and requires advanced solutions. Approaches to handling motion artifacts include: (1) reducing artifacts at the sensor level [26], (2) post-processing the signals using multisensory methods such as accelerometers [27], or (3) deriving useful information directly from the signal [27]. This research combines EBI signal acquisition techniques with custom

algorithms for HR estimation from the forearm, while also considering efforts to capture hemodynamic data from peripheral sites like the carotid, posterior tibial, and brachial arteries [28–30], accounting for both noisy and high-quality signals in algorithm development.

Signal processing is a crucial component, especially in wearables. While it is typically focused on photoplethysmography (PPG) sensors, where the signal quality is higher [31], applying it to EBI signals poses a significant challenge and remains a relatively underresearched area [30,32,33]. Traditionally relying on peak detection [34], the preprocessing stage is of paramount importance [35]. Although the dynamic properties of heart rate (HR) have been addressed in the literature before [36], there has been less focus on practical, wearable-targeted algorithm development.

The novelty of this paper lies in two key aspects:

1. The evaluation of bipolar EBI measurement electrode system configurations (and electrode dimensions) for pulse wave acquisition from the wrist.
2. The development of an approach and algorithm for HR estimation from EBI signals acquired from the wrist.

The combination of signal acquisition methods (e.g., electrode placements and configurations) and signal processing techniques is expected to improve the accuracy of HR and cardiovascular parameter extraction. The proposed approach introduces advances in preprocessing, including baseline removal, normalization, and cross-correlation. It is tested on EBI pulse signals of varying quality measured from the wrist, including signals acquired by both bipolar and tetrapolar electrode EBI configurations. The results help to identify electrode configurations suitable for practical applications. Specifically, we demonstrate that certain bipolar configurations can achieve similar signal-to-noise ratios (SNR) to the more widely studied tetrapolar setups. This has practical significance as the wearable devices with bipolar electrode setups are more robust (as the number of required skin-to-electrode contacts is reduced) and less cumbersome to wear.

2. EBI Measurements

Heart activity is mainly reflected by two physiological parameters: blood flow through veins and arteries and spatial changes in blood dilation of blood vessels. This causes changes in the measured total tissue impedance $Z(t)$, represent as $Z(t) = Z_0(t) + \Delta Z(t)$ (Figure 1). In the content of this research, where the 100 kHz source frequency is utilized, these changes are in fractions of Ohms. The EBI value reflects the changes in blood flow between the measuring electrodes. The decrease in impedance appears when the pulse wave arrives (creating a rapid drop in the signal). Based on the systolic peaks in the EBI waveform, we can determine the HR [37].

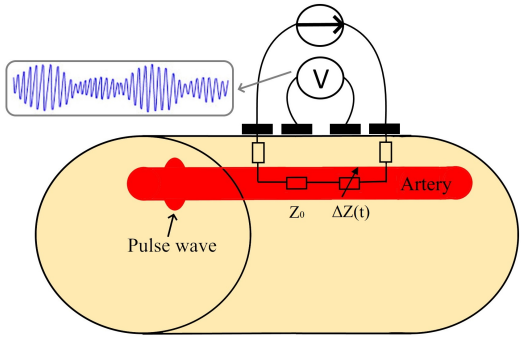


Figure 1. Origin of the pulse wave-related change in the case of measuring EBI of a single artery, illustrating the pulse wave as a bubble of blood.

Figure 1 represents a tetrapolar electrode system for EBI measurements, where the arriving pulse wave with the attendant increase of blood volume causes amplitude modulation in the measured impedance values. The mathematical notations, shown in Figure 1, are presented in detail by the equations in the following subsections of this chapter. This

section introduces the utilized measurement devices and describes the method and the applied setup.

2.1. Measurement Devices

The signals were acquired using an impedance analyzer MFIA of Zurich Instruments AG (Zurich, Switzerland). This device enables two- and four-electrode impedance measurements at up to a frequency of 5 MHz and is supplied with two analog auxiliary and two digital inputs [38].

Monitoring electrodes 2228 of 3M (Maplewood, MN, USA) were used for EBI signal acquisition. PPG signal was picked up using the PulseSensor of World Famous Electronics LLC (New York, NY, USA).

2.2. Measurement Method and Setup

The forearm is a classical location of the wristwatch, which is highly suitable for a wearable biomedical signal monitoring device—targeted in this research. The electrode configurations for comparison were selected by the following criterion:

1. Electrode system: bipolar or tetrapolar;
2. Electrode placement: perpendicular or distal relative to the forearm (radial and ulnar arteries).

We reduced the original electrode dimensions by cutting it into two widths, i.e., 10 mm and 17 mm (Figure 2), to evaluate the effect of electrode-skin contact area size and distance between the electrodes. The initial reason for such a modification was to reduce the electrode width by removing its foam side areas (adhesive and nonconducting) to gain higher density on the restricted wrist area. The experiments were performed with two alternative electrode widths (Figure 2):

1. Original sticky conductive gel area width (17 mm);
2. Width reduced to the diameter of the electrode metal snap (10 mm).

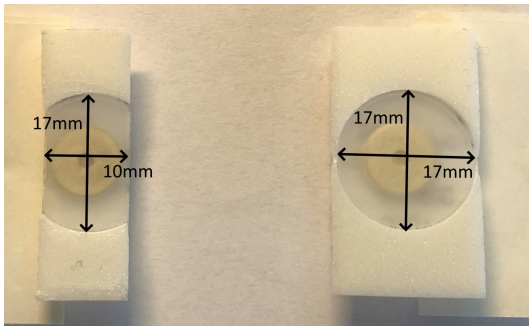


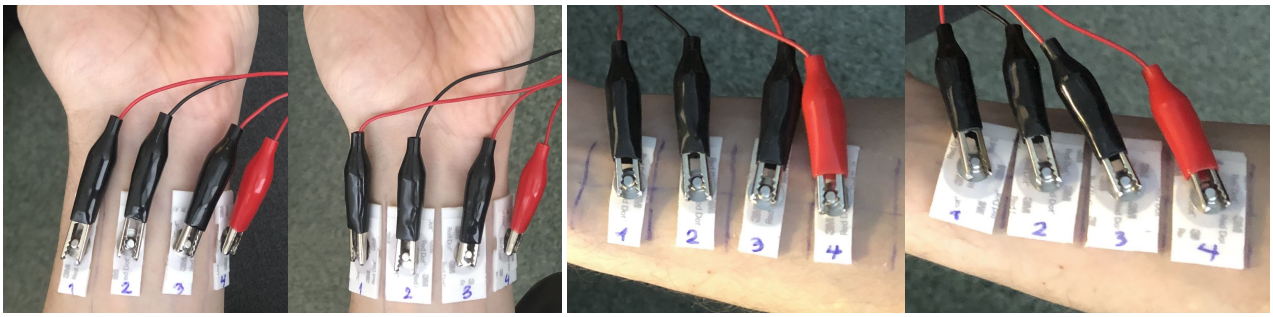
Figure 2. Electrode contact area sizes (10 mm width on the left and 17 mm width on the right).

Positioning of the electrodes with the 17 mm width on the wrist was performed based on the following criteria:

1. We marked the radial artery location with a line on the wrist surface, and two electrodes were attached so that the marked line remained in between these electrodes;
2. The third and fourth electrodes were attached similarly regarding the location of the ulnar artery.

In the case of 10 mm width electrodes, the locations of both arteries remained in between the electrodes, just with a wider gap.

Electrode locations on the forearm in the cases of perpendicular and distal electrodes of both widths are visible in Figure 3a–d)). The distance between the electrodes was 7 mm in the case of narrower electrodes (10 mm) and 1 mm in the case of wider electrodes (17 mm). Simultaneously with EBI measurements, we acquired the PPG from the tip of the index finger.



(**a**) (**b**) (**c**) (**d**)

Figure 3. Chosen electrode placements on the forearm: perpendicular placement of electrodes with 10 mm width (**a**) and with 17 mm width (**b**); distal placement of electrodes with 10 mm width (**c**) and with 17 mm width (**d**).

Ten electrode configurations were defined, of which eight were based on bipolar and two on tetrapolar electrode systems (Table 1).

Table 1. Electrode configurations and dimensions for EBI measurement.

Conf.	System	Contact Area Size	Exc. Electrodes	Meas. Electrodes
A-b10	Bipolar	10 mm	2 and 3	
B-b10	Bipolar	10 mm	1 and 4	
C-b10	Bipolar	10 mm	1 and 3	
D-b10	Bipolar	10 mm	1 and 2	
A-b17	Bipolar	17 mm	2 and 3	
B-b17	Bipolar	17 mm	1 and 4	
C-b17	Bipolar	17 mm	1 and 3	
D-b17	Bipolar	17 mm	1 and 2	
E-b10	Tetrapolar	10 mm	1 and 4	2 and 3
F-b17	Tetrapolar	17 mm	1 and 4	2 and 3

For measuring the EBI ($Z(t)$), the excitation signal with the frequency of 100 kHz and amplitude of 300 mV was used in all the cases. These values fall into the classical ranges for EBI signal acquisition, shown to provide optimal performance properties [39].

Three volunteers (healthy males in their thirties) were used during the measurements in the case of EBI measurements by using the bipolar electrode system. In the case of the tetrapolar electrode system (included for comparison, involving a single volunteer (a healthy male in their thirties)). The measurement protocol is listed subsequently:

1. The volunteer sits comfortably on the chair while the left arm is resting on the armrest;
2. The locations of the radial and ulnar artery are determined by palpation;
3. Electrodes are attached to the skin surface in the desired configuration (concurrently to the PPG sensor on the index finger);
4. Acquisition of the signals (EBI and PPG) (three minutes considered for settling time of electrodes)—while three consecutive measurements were performed in each configuration.

We applied all the ten electrode configurations in both placements: perpendicular and distal.

The initial signal analysis was performed in LabView, firstly by using the Savitzky–Golay filter at side points of 5 and then by determining the $\Delta Z(t)$ from the signal waveforms. $\Delta Z(t)$ is an indicative variable, characterizing the modulation caused by the pulsating flow of blood in the measured signal of EBI (Figure 4), expressed as Equation (1) :

$$Z(t) = Z_0(t) + \Delta Z(t), \quad (1)$$

where $Z_0(t)$ represents the invariable impedance and $Z(t)$ indicates the total measured impedance (Figure 1).

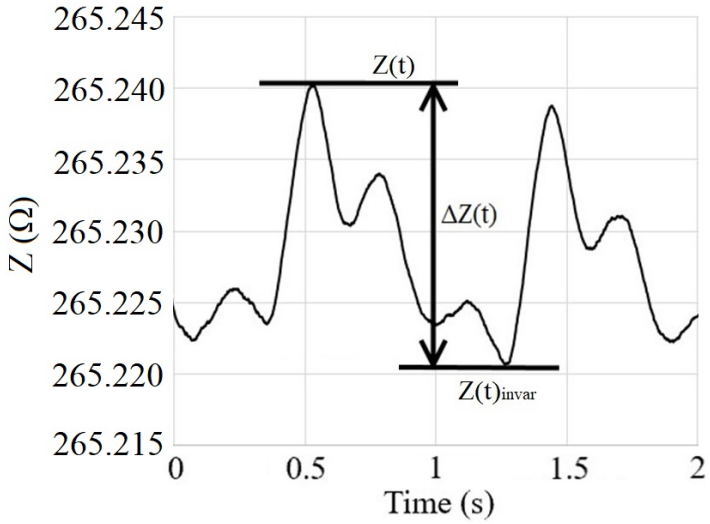


Figure 4. EBI-based pulse waveform with illustrated definition of the modulation depth.

Based on $\Delta Z(t)$ and $Z(t)$, the sensitivity S can be found, designating the depth of the modulation on the carrier signal relative to its maximum value (2):

$$S = (\Delta Z(t) \cdot 100)/Z(t). \quad (2)$$

The experiments involving human participants, as described in this paper, strictly adhere to the principles outlined in the Declaration of Helsinki (1975), as revised in 2013. The noninvasive measurements were conducted following best practices and the authors' expertise. The study was approved by the Life and Medical Sciences Research Ethics Committee of the University of Latvia (protocol number 71-35/160).

3. EBI Signal Processing and Algorithm Development for HR Estimation

This section outlines a method for estimating a person's HR from EBI signals. The method consists of several parts involving preprocessing of the signal, frequency analysis, peak detection, and outlier handling.

We analyzed two ways of signal preprocessing to remove the noise and the baseline variation, the classical band-pass filter (BPF) and, as recently proposed in [33], the Hankel Matrix-based filtering. As a result, we assessed which preprocessing approach gives more accurate HR estimation.

This algorithm is implemented in the MATLAB R2023b environment, utilizing certain built-in functions in a novel way to improve the precision of HR (BPM) calculation by performing the following steps (the respective flow diagram is visible in Figure 5):

1. Preprocessing:
   (a) BPF [40];
   (b) Baseline removing using Hankel Matrix [33].

   Differences between a signal filtered with BPF and Savitzky–Golay filters can be seen in Figure 6.
2. Normalization.
3. First HR estimation using Cross-correlation [41].
4. Accurate HR estimation by peak detection.

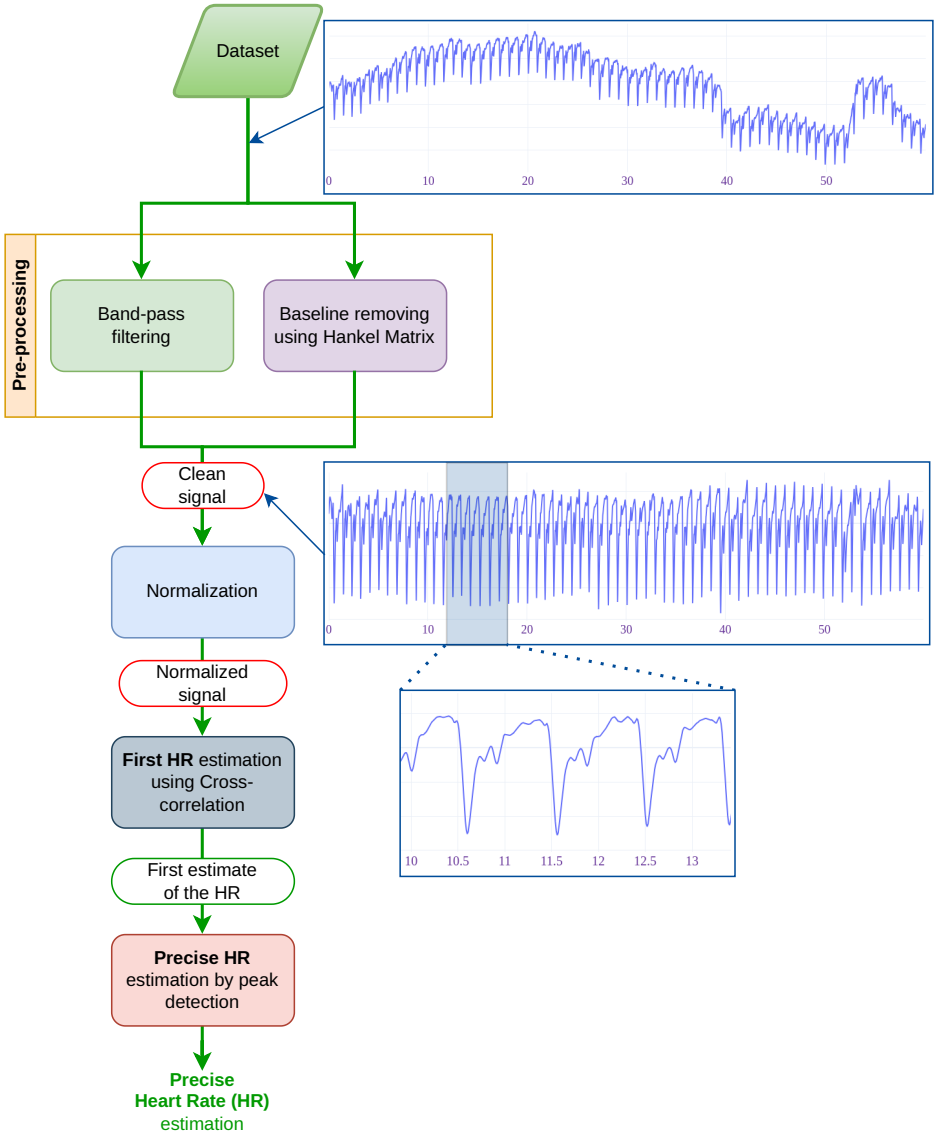


Figure 5. Flow diagram describing the data processing steps for accurate heart rate estimation.

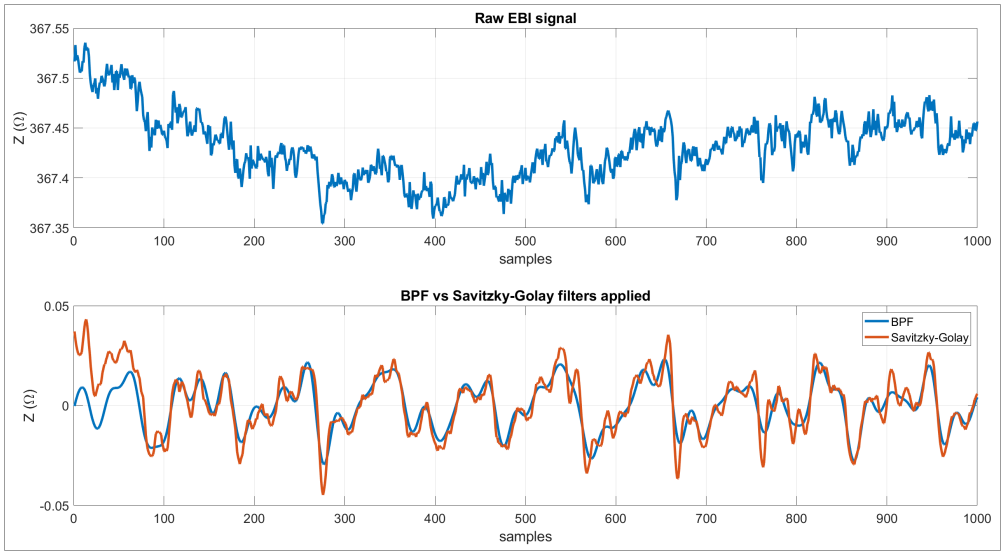


Figure 6. The raw EBI signal (**top panel**) and the results after applying a band-pass and a Savitzky–Golay filter (**the bottom panel**).

3.1. Preprocessing as Band-Pass Filtering

In the present experimental context, EBI data were acquired over approximately one minute (with a source frequency of 100 kHz), and the sampling rate is 100 samples per second. PPG was acquired concurrently to establish a congruent ground truth dataset of equal length. The EBI measurements utilize the real part of the complex impedance, encompassing the absolute impedance value, noise, and the inherent cardiac activity embedded within the signal. Different filtering methods are required to obtain the heartbeat from the signal. The noise component of the measured EBI signals is removed using a BPF. The filter's settings were established based on a frequency response range, determined using the upper and lower limits of the HR, assuming that these limits were unattainable. We designed the filter in $Matlab^{TM}$ filter designer using the parameter band-pass infinite impulse response (IIR).

The filtered signal is obtained via a zero-phase filtering approach to avoid phase distortion. For this, the Matlab function filtfilt(x) is used [40], which processes the input data x in both the forward and reverse directions:

$$\mathbf{x}_{\text{filt}}(t) = \text{filtfilt}(\text{H}, \mathbf{x}(t)), \tag{3}$$

where $\mathbf{x}(t)$ is the input signal as a function of time t, H represents the filter's transfer function, and $\mathbf{x}_{\text{filt}}(t)$ is the filtered signal.

- Filter type: IIR filter;
- The first stop-band: lower frequency edge = 0.1 Hz, attenuation = 10 dB;
- Pass-band: frequency edges = [0.5 5.0] Hz;
- The second stop-band: upper frequency edge = 6 Hz, attenuation = 10 dB.

We employed the elliptic filter design method to create a filter, with the MatchExactly parameter ensuring precise alignment with pass-band frequencies. The signal, set at a constant 100 samples per second, undergoes band-pass filtering for HR estimation, eliminating DC, low, and high-frequency noise.

3.2. Preprocessing Using Hankel Matrix-Based Approach

Typically, breathing and slow-motion artifacts are eliminated by applying a high-pass (or BPF) filter to the input signal in the time domain. Another approach could be fitting a low-order polynomial to the input signal and subtracting the fitted mean line from the original signal.

In our previous research, we have developed a Hankel matrix-based solution [33] for constructing three cardiac periods and sliding these through the signal, thus allowing online and real-time signal filtering. In the current paper, a simplified version of the Hankel matrix-based filtering approach is used for offline processing, converting the entire signal into the Hankel matrix. A short description of the algorithm is given below:

1. Estimate averaged cardiac frequency (HR) for the full signal using FFT.
2. Define the size of Hankel matrix columns equal to the averaged cardiac period (in samples).
3. Construct the Hankel matrix for the full signal.
4. For each matrix column: apply mean() function to the column and replace all the column values with the estimated mean value (use of the mean() function allows to estimate the *mean line* of the signal, in turn, applying, e.g., min() function to each column estimates the *base line* of the signal and, respectively, use of max() function, estimates the *peak line* of the signal. In the current work, we used the *mean line* estimation approach).
5. Apply the *hankelization* procedure to the matrix—this means to change, individually, each anti-diagonal of the matrix to the same value. In our approach, we use anti-diagonal averaging by mean values. For each anti-diagonal, the mean value is

estimated, and all elements of the corresponding anti-diagonal are replaced by the found mean value.

6. Transform the obtained (*filtered*) Hankel matrix to the resulting filtered baseline signal.
7. Finally, subtract the obtained in the previous step the baseline from the input signal. The result of this step is a filtered cardiac signal $\mathbf{x}_{\text{filt}}(t)$.

3.3. Signal Normalization

Subsequently, after the filtering, the signal is normalized using Equation (4):

$$\mathbf{x}_{norm}(t) = \frac{\mathbf{x}_{\text{filt}}(t) - \text{mean}(\mathbf{x}_{\text{filt}}(t))}{\max(\mathbf{x}_{\text{filt}}(t)) - \min(\mathbf{x}_{\text{filt}}(t))}, \tag{4}$$

where $\mathbf{x}(t)$ is the signal vector, $\mathbf{x}_{\text{filt}}(t)$ is filtered version of the signal, $\min()$, $\max()$, and $\text{mean}()$ are functions, which estimate the minimum, maximum, and mean values, respectively, of the $\mathbf{x}_{\text{filt}}(t)$.

3.4. Cross-Correlation for BPM Estimation

Cross-correlation was selected because it is a robust method for detecting periodic patterns in noisy, nonstationary signals [42], making it particularly well-suited for EBI-based HR estimation. EBI signals can be prone to interference from motion artifacts, physiological noise, and other environmental factors, which can obscure the HR signal. Cross-correlation helps mitigate these issues by comparing the acquired signal to a reference template or waveform, such as a clean heartbeat signal, to identify matching periodic features.

This method enhances the accuracy of HR estimation for several reasons:

1. Noise Resilience: Cross-correlation emphasizes similarities between the signal and the template, reducing the impact of random noise or artifacts that do not follow the expected periodic pattern of heartbeats.
2. Pattern Matching: Even when the signal is distorted, cross-correlation can still detect the presence of periodicity by identifying recurring patterns, ensuring that heartbeats are correctly identified even under suboptimal conditions.
3. Range Selection: Particularly suited for cardiac signals, cross-correlation can be targeted to a specific frequency range (e.g., 0.5 to 5 Hz), which encompasses the HR range. This targeted approach reduces unwanted processing and optimizes computational efficiency by focusing only on the relevant frequency band.

After preprocessing, we pass the signal to a function that determines HR. HR estimation consists of two main parts: the cross-correlation part and the peak detection part. The Cross-Correlation method [41] for BPM estimation from the EBI signal is performed as follows: the input signal is divided into multiple equal parts M (10 parts for this signal). The signal is divided into parts based on its time constant and the duration according to Equation (5):

$$\text{duration} = \frac{\text{length(in_signal)}}{\text{fs}}, \quad \text{num_parts} = \left\lfloor \frac{\text{duration}}{\text{time_constant}} \right\rfloor \tag{5}$$

where the *time_constant* is selected between 2 and 4 s, optimizing the segmentation of the input signal for effective analysis.

For each segment, frequencies between 0.5 Hz and 5 Hz are tested to identify the one that best correlates with the EBI signal, using sinusoidal generation and cross-correlation, as shown by Equations (6) and (7) :

$$\sin_a(t_i) = \sin(2\pi f t_i), \tag{6}$$

$$\rho(X, Y, k) = \sum_{n=0}^{N-k-1} X[n] \cdot Y[n-k]. \tag{7}$$

where X and Y represent the input signals, k is the lag parameter, which determines the time shift between the two signals, and N is the greater of the lengths of X and Y. The equation calculates the similarity between X and Y as Y is shifted relative to X. Positive values indicate a positive correlation, while negative values indicate a negative correlation. In this example, the correlation between input EBI signal X_i and generated sine signals $\sin_a(f)$ are calculated.

The frequency with the highest correlation is considered to support the effective monitoring of temporal variations in HR, closely approximating the best frequency for each part Equations (8)–(10). If the current frequency has a higher correlation, i.e., if the following is true:

$$\theta_i(f) > max :_{\theta_i}, \tag{8}$$

where

$$max :_{\theta_i} = \theta_i(f) \tag{9}$$

and

$$\hat{f}_i = f, \tag{10}$$

then, convert the best frequency to BPM and store it as Equation (11):

$$BPM_i = \hat{f}_i \cdot 60. \tag{11}$$

Thereafter, calculate the mean BPM of all the best BPM values and update BPM values that deviate from the mean significantly. Then, calculate the difference from the mean BPM Equation (12):

$$\delta_i = |BPM_i - B\hat{P}M|. \tag{12}$$

If the difference is greater than the threshold, e.g., if Equation (13):

$$\delta_i > \theta, \tag{13}$$

then set Equation (14):

$$BPM_i = B\hat{P}M. \tag{14}$$

The signal is divided into frames of length:

$$window_{size} = round\left(\frac{fs}{\hat{f}}\right) + 1. \tag{15}$$

3.5. Accurate HR Estimation by Peak Detection

After the correlation is performed to the whole spectrum in all defined segments of the waveform to determine the best frequency, the maximum value is located along with the best frequency.

To improve BPM estimation accuracy, BPM values that deviate from the median BPM by more than a defined threshold are set to the median BPM.

Next, the window-based peak detection is performed: the EBI signal is divided into smaller windows as shown in Figure 7 (upper plot) (of a certain length obtained from the cross-correlation method, according to Equation (15) to determine the peaks in each window corresponding to heartbeats EBI value drops).

Within each window, the peak (maximum value) is detected, and the time of the event is stored as seen in Figure 7 (bottom plot). From the detected values (peaks and peak locations or indices), location values are subsequently calculated into BPM, see in Equation (16):

$$BPM_i = \frac{60}{\Delta t}, \tag{16}$$

where Δt represents the time difference between peak locations.

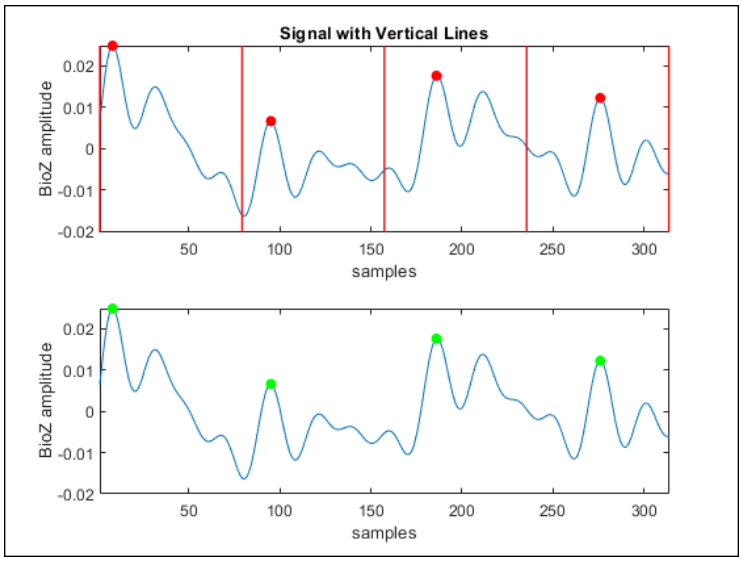


Figure 7. Example of EBI signal partition for the window-based peak detection (**upper plot**) and the peaks of the detected pulse waves (**bottom plot**).

The window for processing the EBI signal is defined by subtracting one from the window size, calculated as shown in Equation (15). This adjustment ensures the window spans from the starting index 'i' to 'end'. Within each window, we identify the maximum peak value (maxPeak) and its index (maxIndex). The determination of the peak time (t_{peak} in seconds) is carried out according to Equation (17):

$$t_{peak} = \frac{i + maxIndex - 3}{f_s}. \tag{17}$$

Then, we perform the BPM value determination using the peak location time intervals. To estimate the instantaneous HR (in BPM), we analyze the time intervals between consecutive peak locations. The BPM is calculated by dividing 60 by the time difference between peak locations, as illustrated by Equation (16).

Then, we proceed with the computation of the median BPM (BPM_{meidan}) and the Median Absolute Deviation (BPM_{MAD}) of BPM values using the predefined functions available in the standard Matlab library. An outlier threshold is established as a constant $\theta_{outlier}$ = 3, and the final BPM is determined using Equations (18) and (19). If:

$$|\delta_i - BPM_{median}| > \theta_{outlier} \cdot BPM_{MAD}, \tag{18}$$

then:

$$BPM_i = BPM. \tag{19}$$

The collected data underwent diverse analytical assessments. The PPG signal was subjected to the 'findpeaks' algorithm (MATLAB), establishing thresholds to identify signal peaks, albeit potentially misinterpreting them as heartbeats. Precision was augmented by meticulously adjusting the 'findpeaks' function parameters, specifically "minPeakDistance" and "minPeakProminence" for each PPG signal. This manual fine-tuning aimed to visually achieve the highest accuracy in results. The EBI signal underwent processing using the 'findpeaks' method and a newly developed algorithm called 'BPM DL'. Figure 8 shows the processed BPM data using the described methods.

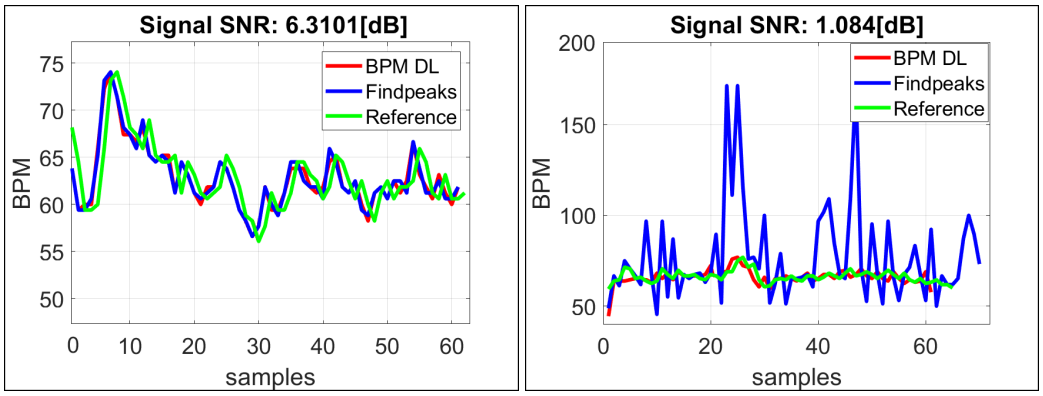


Figure 8. Examples of calculated BPM variations from good quality (high SNR) electrical bioimpedance (EBI) signals (**left plot**) and calculated BPM values from noisy (low SNR) EBI signals (**right plot**) while using the PPG signals for reference information.

In summary, this algorithm estimates the BPM by first identifying the best frequency that correlates with the EBI signal using cross-correlation and then detecting peaks in the signal to estimate the HR more accurately. Finally, it calculates BPM based on the time differences between peak locations. The result is expected to provide an accurate estimation of the HR from the EBI signal.

4. Results

This section presents the EBI measurements from the wrist by utilizing the predetermined electrode configurations and the developed HR estimation algorithm comparison with the reference method.

Figure 8 serves as an illustrative comparison of BPM calculations made according to Equation (16) by two different methods. The left shows the better and stable results with high SNR value driven by the 'findpeaks' algorithm (shown as blue line) compared to the ground truth reference (indicated by a green line—PPG signal). Meanwhile, the newly developed algorithm presented in this work—'BPM DL'—represented by the red line, provides the output through direct peak detection.

The use of a stationary algorithm for heart rate estimation becomes impractical in conditions where the 'findpeaks' method produces unstable and imprecise cardiac activity information with significant outliers (right side of Figure 8 with a much lower SNR). The appearance of spurious peaks significantly affects the accuracy of the heart rate signal, resulting in variability that differs from the actual values. Conversely, the 'BPM DL' algorithm maintains visibly stable results (depicted by the red line) that adhere closely to the ground truth (green line), reinforcing its potential utility in noisy environments. The blue and green lines coincide, but the red one deviates—this is because the EBI signal is measured from the wrist and the ground truth from the fingertip (presenting a delay).

4.1. Measurement Results

The acquired signals of EBI and PPG were sampled with a frequency of 128 Hz, which is enough to restore the biomedical heart activity-related signal.

The calculated mean values of $\Delta Z(t)$ together with the standard deviations (SD) (σ) are visible in Table 2.

Table 2. Calculated mean values of $\Delta Z(t)$ in the cases of the chosen electrode configurations.

Conf. No.	$\Delta Z(t)_{mean} \pm \sigma(\Omega)$	
	Perpendicular Placement	**Distal Placement**
A-b10	0.031 ± 0.0020	0.089 ± 0.0096
B-b10	0.090 ± 0.0039	0.198 ± 0.0406
C-b10	0.053 ± 0.0055	0.163 ± 0.0122
D-b10	0.045 ± 0.0021	0.122 ± 0.0144
A-b17	0.020 ± 0.0020	0.147 ± 0.0191
B-b17	0.060 ± 0.0017	0.213 ± 0.0156
C-b17	0.046 ± 0.0028	0.194 ± 0.0070
D-b17	0.032 ± 0.0033	0.134 ± 0.0173
E-t10	0.025 ± 0.0005	0.037 ± 0.0048
F-t17	0.019 ± 0.0010	0.039 ± 0.0026

The calculated mean values of *S* are visible in Figure 9.

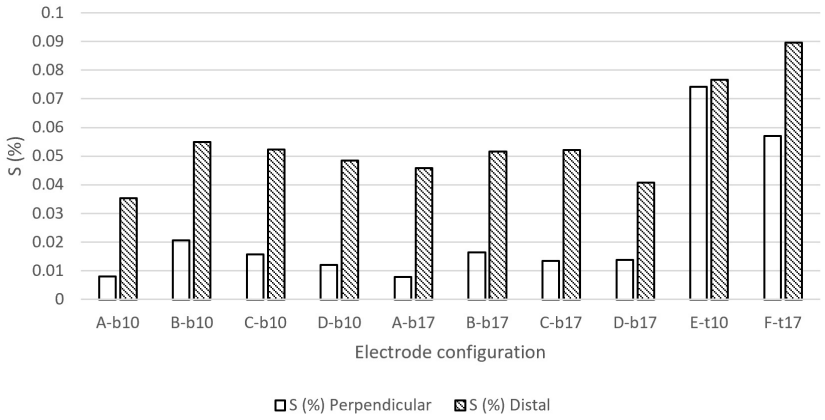


Figure 9. Calculated mean values of S in the cases of the chosen electrode configurations.

4.2. Signal Processing Results

4.2.1. Signal-to-Noise Ratio Calculation

A detailed description of the method that we use to estimate the quality of EBI signals can be found in [23]. To summarize the main steps of the method, it works as follows:

1. The continuous wavelet transform is carried out on the measured signal.
2. Wavelet ridges are identified.
3. Both energy and duration of wavelet ridges are computed and normalized to the total energy and duration of the measured signal.
4. Obtaining the weighted ridge energy by multiplying both quantities from step 3.
5. Median filter is applied to the weighted ridge energy to estimate the extent of noise.
6. Finally, an SNR is calculated as a ratio of squared weighted ridge energy summed over all ridges divided by the estimated signal noise. SNR is expressed in decibels through the log10 transformation.

4.2.2. Calculation of BPM Differences

The differences between the BPM estimates from each method and the reference are calculated as follows Equation (20):

$$\mathrm{DIFF}_{\mathrm{BPM}} = \mathrm{mean}(\mathrm{BPM}_{\mathrm{method}}) - \mathrm{mean}(\mathrm{BPM}_{\mathrm{reference}}), \quad (20)$$

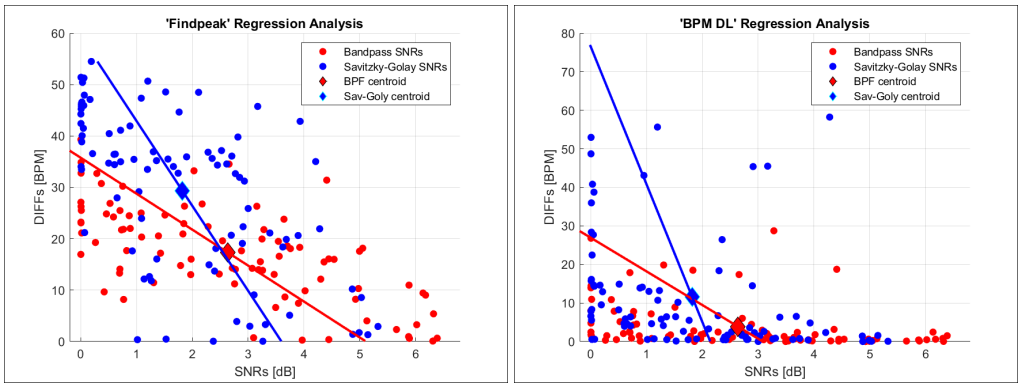
where $\mathrm{BPM}_{\mathrm{method}}$ represents the BPM estimates from one of the input signals and $\mathrm{BPM}_{\mathrm{reference}}$ is BPM estimated from a reference or ground truth signal (PPG).

4.2.3. Connection Between SNR and BPM Differences

The scatter plots shown in Figure 10a,b depict the BPM differences against the SNR values for two signal processing methods—the newly developed 'BPM DL' and the MATLAB's built-in function 'findpeaks', each applied using both BPF and Savitzky–Golay filters. The BPM differences are calculated according to Equation (20), while the calculation of SNR values is described in [23]. Ideally, a higher quality EBI signal would result in smaller differences between the BPM values obtained as the BPM difference from the EBI and PPG (ground truth) signals.

In order to quantitatively compare BPF and Savitzky–Golay filtering methods, the centroid of the point cloud in the SNR-BPM difference plane was calculated for both filtering methods. These centroids provide an indication of the overall performance trend within each dataset, allowing for easier comparison between filtering techniques (shown as a diamond symbol in Figure 10). Also, a linear regression line has been added to each dataset to illustrate their respective trends.

The centroid of the band-pass filter with the 'BPM DL' method shows a BPM difference of 4.18 and an SNR of 2.61 dB, demonstrating its superior accuracy. In comparison, the 'findpeaks' method with the same filter has a BPM difference of 17.30, which is more than four times worse despite having a nearly identical SNR of 2.63 dB. When using the Savitzky–Golay filter, the 'BPM DL' method again performs better, with a BPM difference of 11.51 and an SNR of 1.8 dB. However, the 'findpeaks' method exhibits a much larger BPM difference of 29.37, making it more than two and a half times less accurate, with a similar SNR of 1.81 dB. These results clearly indicate that the 'BPM DL' method consistently outperforms 'findpeaks', especially in terms of BPM accuracy, regardless of the filtering technique used.



(**a**) (**b**)

Figure 10. Signal quality estimation results shown as a scatter plot in BPM difference—SNR plane for both signal filtering methods—band-pass signal and Savitzky–Golay. (**a**) The 'findpeaks' BPM estimation method; (**b**) the 'BPM DL' BPM estimation method. Diamond symbols show centroids of point clouds for both filtering methods and straight lines show the fitted linear regression model according to the color of each dataset.

We conducted a parametric study to assess the SNR value of the measured EBI signal at different electrode configurations in both bipolar and tetrapolar setups (the results as a colormap in Figure 11). Electrode placements, such as 1-2, 1-3, 1-4, 2-3, and 1-2-3-4, correspond to the specific electrode configurations depicted in Figure 3 and Table 1. The SNR values were calculated for signals that were processed using the BPF (letter B in Figure 11) and Savitzky–Golay (letter S in Figure 11) filters, prior to applying the 'findpeaks' and 'BPM DL' algorithms.

Figure 11 provides a clear visualization of which electrode configurations yield the best and worst results across all test subjects and repeated measurements. The lowest SNR values manifest in bipolar configurations A-b10 and A-b17 for all test subjects and electrode sizes. The best results in the bipolar setup manifest using the configuration B-b10 (Table 1).

The best results are achieved in tetrapolar configuration with band-pass filtering, illustrated for BPM differences and MAPE values in Figures 12 and 13, respectively.

Test setup			Bipolar								Tetrapolar	
	Test	El.conf	1-2		1-3		1-4		2-3		1-2-3-4	
Dataset	subject	size (cm)	B	S	B	S	B	S	B	S	B	S
1	1	1	0.004	0.045	0.002	0.012	4.996	2.77	0.524	0.01	6.18	5.03
		1.7	0.701	0.595	0.695	0.604	3.541	2.522	0.287	0.01	3.097	2.375
	2	1	1.977	1.745	3.901	2.697	4.019	1.263	0.419	0.069	5.128	3.743
		1.7	0.702	1.201	2.281	1.357	5.883	3.895	2.756	0.017	5.875	3.309
	3	1	3.072	1.042	2.481	2.707	4.36	3.683	0.004	0.165	3.248	2.397
		1.7	0.003	0.5	4.54	4.21	2.54	2.816	0.585	0.004	3.281	1.23
2	1	1	2.716	1.762	1.429	0.713	0.822	1.084	0.368	0.003	6.31	3.263
		1.7	0.015	0.023	0.868	0.003	1.97	1.66	0.009	0.01	3.968	1.528
	2	1	3.493	1.362	3.659	1.135	4.924	3.621	0.767	0.211	4.445	1.015
		1.7	1.846	1.562	3.641	2.449	4.977	4.282	0.763	0.001	5.658	4.875
	3	1	3.757	2.932	1.391	1.3	6.134	3.105	0.002	0.188	3.466	3.029
		1.7	4.301	3.931	0.729	0.65	2.657	3.17	2.175	1.52	4.408	2.896
3	1	1	1.508	0.063	1.09	0.952	2.77	2.354	$5{\cdot}10^{-4}$	0.02	6.021	2.796
		1.7	0.459	0.03	0.886	1.194	3.155	1.896	0.262	0.052	6.388	5.145
	2	1	1.306	0.923	3.218	2.421	4.445	2.298	1.081	0.006	6.322	5.326
		1.7	1.788	0.618	3.556	3	3.924	2.909	1.858	0.713	5.89	4.989
	3	1	3.186	2.281	0.002	0.882	3.702	3.388	0.005	0.056	5.053	4.866
		1.7	2.88	2.615	3.258	2.847	0.752	0.508	2.029	2.111	1.83	1.089
Mean			**1.873**	**1.29**	**2.09**	**1.618**	**3.643**	**2.624**	**0.772**	**0.287**	**4.809**	**3.272**

Figure 11. SNR [dB] colormap across all electrode configurations for three test subjects. The table visualizes SNR where higher values are in green and lower values in red (with a gradient transition for intermediate values between these extremes).

It is evident in Figure 11 that the SNR values vary significantly between the configurations, particularly when BPF is applied. For example, configurations 1-3 and 1-4 show higher SNR values, suggesting a more accurate measured signal in Bipolar electrode setup. In the Savitzky–Golay filter case, the SNR decreases compared to the BPF. While both filters can improve signal clarity, the BPF is generally more effective in enhancing SNR. The variation in SNR across placements highlights the importance of electrode configuration for optimal EBI measurements.

Similar to the SNR values shown earlier, Figure 12 illustrates the BPM differences. While SNR values focus on the effects of signal preprocessing and filtering, Figure 12 depicts the overview layout of algorithm performance on the proposed BPM processing methods. Results from the 'findpeaks' and 'BPM DL' algorithms are shown separately for clarity.

BPM difference is a critical metric that reflects the discrepancy between the BPM calculated by the algorithm and the ground truth value (PPG). The figure uses the label "BPM" to maintain consistent units. Larger deviations from the ground truth indicate poorer HR estimation accuracy for the given electrode configuration.

In Figure 12, generally, the 'BPM DL' method tends to produce more accurate BPM estimates, with smaller differences from the ground truth in several configurations. For configurations such as 1-2 and 1-3, the differences in BPM using 'BPM DL' are often close to zero or minimal, sometimes as low as 0.059 or 0.467 BPM, reflecting high accuracy. In contrast, the 'findpeaks' method shows significantly higher deviations, often exceeding 10 BPM (e.g., configuration 1-3 with 76.97 BPM deviation, indicating poorer performance).

Findpeak method												
Test setup			Bipolar								Tetrapolar	
Dataset	Test subject	El.conf size (cm)	1-2		1-3		1-4		2-3		1-2-3-4	
			B	S	B	S	B	S	B	S	B	S
1	1	1	26.27	41.5	23.24	33.49	17.57	32.68	26.88	45.81	9.029	8.559
		1.7	14.1	36.42	13.3	34.42	19.49	37.16	32.71	46.08	0.736	0.052
	2	1	16.02	32.76	7.447	20.68	9.87	11.83	9.662	21.2	4.021	5.112
		1.7	25.49	50.67	22.36	35.2	10.97	20.63	11.22	38.87	0.952	3.303
	3	1	14.24	29.16	13.13	36.09	15.49	19.87	32.77	47.11	19.95	13.71
		1.7	23.09	34.72	15.99	35.03	19.6	39.8	24.24	34.04	21.78	12.64
2	1	1	14.3	44.66	17.19	34.99	17.69	47.36	30.75	51.42	0.092	0.053
		1.7	21.12	40.06	24.48	42.43	13.02	34.06	25.52	46.28	0.272	0.466
	2	1	6.626	16.05	8.663	12.16	8.224	18.39	8.187	36.57	0.379	0.356
		1.7	22.95	35.51	23.8	34.34	10.31	21.93	21.84	44.27	2.333	1.395
	3	1	18.08	31.22	20.55	36.94	9.439	9.078	39.31	54.51	13.06	2.972
		1.7	12.14	42.85	21.73	27.97	34.53	45.76	26.77	48.57	31.41	19.09
3	1	1	24.62	47.95	20.33	35.45	14.05	35.63	16.96	46.6	3.265	3.895
		1.7	24.84	50.43	22.01	33.5	26.32	35.94	19.27	45.93	0.65	1.324
	2	1	11.46	17.63	15.53	18.11	16.07	14.93	25.01	45.28	5.391	2.929
		1.7	14.79	36.48	16.59	25.89	18.33	22.34	26.34	41.12	0.608	1.729
	3	1	13.98	36.84	27.11	41.95	18.59	21.12	34.88	51.28	18.15	10.21
		1.7	17.66	34.55	13.86	31.95	30.22	40.46	33.23	48.5	20.93	23.95
Mean			**17.88**	**36.64**	**18.18**	**31.7**	**17.21**	**28.28**	**24.75**	**44.08**	**8.5**	**6.208**
STD			**5.714**	**9.543**	**5.534**	**7.939**	**7.195**	**11.8**	**8.9**	**7.681**	**9.827**	**7.056**
BPM DL method												
1	1	1	1.712	27.71	2.451	5.546	0.059	1.2	5.146	35.98	0.591	0.067
		1.7	17.87	4.68	2.561	3.957	0.158	2.499	1.515	28.37	0.468	0.469
	2	1	1.769	0.477	0.447	2.02	1.781	5.794	7.867	0.594	0.719	0.772
		1.7	2.312	10.71	2.461	6.418	0.286	0.388	1.801	8.319	0.408	0.85
	3	1	2.931	13.02	0.536	1.618	3.147	6.511	7.905	14.61	0.553	1.152
		1.7	26.81	8.223	0.594	2.336	1.139	0.565	2.067	52.97	28.74	13.22
2	1	1	6.017	5.499	1.722	4.038	4.527	76.97	10.87	48.7	0.798	0.64
		1.7	10.95	22.44	1.48	7.886	0.769	2.635	1.544	16.12	0.168	0.129
	2	1	0.003	0.493	0.682	0.7	0.006	0.518	7.794	12.92	0.58	0.527
		1.7	2.765	10.18	1.064	1.657	0.619	58.24	4.284	6.589	0.114	0.008
	3	1	0.357	2.304	1.307	4.129	2.441	2.611	4.779	9.521	1.304	1.49
		1.7	0.15	4.808	0.868	4.562	17.37	45.5	0.273	6.44	18.74	14.47
3	1	1	8.9	14.35	0.787	43.1	1.559	26.44	7.952	0.538	0.461	0.538
		1.7	0.493	40.82	0.11	55.65	2.091	0.674	0.335	14.61	1.498	1.572
	2	1	19.85	14.11	0.209	0.457	0.105	18.38	7.173	15.74	0.032	0.064
		1.7	1.347	5.88	0.44	0.019	0.27	45.39	0.02	6.389	0.129	0.313
	3	1	1.432	6.702	13.94	13.89	2.379	6.315	14.48	38.76	0.256	1.416
		1.7	4.452	4.182	0.769	3.598	6.679	14.88	2.026	3.272	18.49	4.62
Mean			**6.118**	**10.92**	**1.801**	**8.976**	**2.522**	**17.53**	**4.88**	**17.8**	**4.114**	**2.351**
STD			**7.842**	**10.37**	**3.124**	**15.2**	**4.104**	**23.4**	**4.082**	**16.22**	**8.475**	**4.316**

Figure 12. Absolute BPM estimation errors, as quantified by the $DIFF_{BPM}$ metric. Shows results across all electrode configurations for three test subjects. Higher errors are shown in red and lower differences in green, using a color gradient for values in-between.

Findpeak method												
Test setup			Bipolar								Tetrapolar	
Dataset	Test subject	El.conf size (cm)	1-2		1-3		1-4		2-3		1-2-3-4	
			B	S	B	S	B	S	B	S	B	S
1	1	1	45.6	64.71	39.39	53.69	31.45	50.93	45.9	69.04	15.2	15.31
		1.7	30.06	61.61	29.99	59.18	32.56	60.75	51.85	72.81	5.407	4.682
	2	1	29.23	51.21	17.51	33.98	17.79	19.97	22.07	35.63	10.57	11.8
		1.7	44.67	83.12	38.68	56.27	21.29	33.88	21.19	61.09	6.798	9.506
	3	1	29.43	57.21	27.51	66.66	30.99	39.98	63	90.21	38.25	28.56
		1.7	49.89	67.46	35	68.99	38.85	72.34	47.78	58.72	43.53	28.92
2	1	1	29.61	71.37	30.14	53.9	32.53	77.68	49.42	81.86	1.898	2.301
		1.7	37.72	60.23	47.37	69.79	25.78	56.13	47.77	76.47	2.417	3.34
	2	1	16.39	30.24	18.46	26.46	18.87	32.75	20.56	57.53	3.172	3.203
		1.7	40.36	57.74	39.99	54.84	20.39	34.81	42.01	69.81	6.077	5.368
	3	1	33.42	57.6	39.72	70.21	19.9	19.46	71.1	98.01	25.52	6.666
		1.7	24.93	78.97	41.46	53.31	63.97	83.02	51.99	88.01	59.66	37.37
3	1	1	41.52	77.59	34.01	54.98	29.17	57.73	31.75	69.94	7.198	7.148
		1.7	44.54	78.51	38.54	56.01	45.09	62.14	34.72	73.85	6.989	9.065
	2	1	20.42	28.17	26.12	31.3	27.89	29.1	40.35	68.79	11.02	9.804
		1.7	26.75	57.59	29.73	41.68	35.14	37.71	44.61	64.33	3.652	6.161
	3	1	27.4	66.87	49.69	75.62	36.67	39.94	65.2	89.29	32.9	19.56
		1.7	35.11	61.93	30.81	60.47	56.7	76.72	64.67	92.38	38.18	44.15
Mean			**33.73**	**61.78**	**34.12**	**54.85**	**32.5**	**49.17**	**45.33**	**73.21**	**17.69**	**14.05**
STD			**9.313**	**14.85**	**8.739**	**13.84**	**12.63**	**20.05**	**15.21**	**15.32**	**17.46**	**12.56**
BPM DL method												
1	1	1	23.07	48.45	6.501	19.04	2.631	4.015	32.56	59.52	2.336	1.556
		1.7	31.84	22.44	8.715	10.65	3.013	8.22	34.02	52.81	3.772	2.016
	2	1	6.804	4.897	1.985	5.835	5.103	10.8	23.62	15.27	3.341	2.968
		1.7	28.24	24.78	6.739	14.72	2.33	3.313	20.06	18.83	2.481	2.138
	3	1	19.69	27.12	9.609	11.11	12.64	17.23	26.7	37.81	4.652	15.8
		1.7	60.38	22.02	7.834	6.652	18.54	6.305	26.38	101.1	52.59	33.92
2	1	1	18.68	14.23	7.988	11.43	13.92	121.3	31.76	80.54	2.244	1.646
		1.7	29.13	52.63	8.382	22.6	7.284	11.74	30.37	41.6	2.067	1.81
	2	1	5.257	4.416	4.02	3.444	3.027	3.388	19.26	28.56	2	1.685
		1.7	25.46	25.79	4.368	5.821	3.352	94.39	23.47	17.96	1.31	0.609
	3	1	15.82	10.53	6.367	10.81	12.58	9.821	36.12	31	4.493	5.558
		1.7	22.41	15.94	9.58	16.71	45.44	89.35	12.59	15.93	47.09	29.71
3	1	1	28.33	27.55	6.267	69.9	10.29	46.07	29.85	19.64	1.892	1.982
		1.7	33.92	75.85	11.49	93.02	7.194	6.122	38.31	36.62	3.389	2.896
	2	1	33.57	23	4.271	2.736	3.567	29.43	45.83	37.69	1.376	0.899
		1.7	21.59	15.94	3.321	3.772	3.418	73.29	19.72	19.78	2.757	1.462
	3	1	18.12	17.61	28.05	27.5	10.93	14.89	37.13	73.97	3.081	19.19
		1.7	20.9	17.83	8.601	17.55	22.02	37.1	20.91	17.32	44.5	26.56
Mean			**24.62**	**25.06**	**8.005**	**19.63**	**10.4**	**32.6**	**28.26**	**39.22**	**10.3**	**8.467**
STD			**12**	**17.74**	**5.587**	**23.85**	**10.51**	**37**	**8.375**	**25.16**	**17.46**	**11.22**

Figure 13. Relative BPM estimation errors, as quantified by the MAPE metric. Shows results across all electrode configurations for three test subjects. Higher errors are shown in red and lower differences in green, using a color gradient for values in-between.

4.2.4. Mean Absolute Percentage Error (MAPE)

MAPE is a metric used to evaluate the accuracy of a forecasting or prediction model. It measures the average absolute percentage difference between the predicted and actual values. MAPE is computed using Equation (21):

$$\text{MAPE} = \frac{100\%}{n} \sum_{i=1}^{n} \left| \frac{\text{BPM}_{\text{reference}}[i] - \text{BPM}_{\text{method}}[i]}{\text{BPM}_{\text{reference}}[i]} \right|, \tag{21}$$

where n is the number of comparisons, $BPM_{reference}$ is the BPM estimated from a reference signal (PPG), and BPM_{method} is the BPM estimate from one of the evaluated methods. In the context of this research, MAPE is used to quantify the accuracy of the BPM estimates in relation to the reference signal.

Similar to the previous colormap graphs with a consistent view, Figure 13 shows the calculated MAPE values according to Equation (21). The graph separates the results of the 'findpeaks' and 'BPM DL' algorithms, allowing a detailed comparison of the two methods.

Generally, the 'BPM DL' method consistently produces lower MAPE values, indicating better accuracy in estimating HR. For example, in configurations 1-3 and 1-4, MAPE values for 'BPM DL' are often significantly lower. In contrast, 'findpeaks' can exhibit much larger errors, with MAPE values exceeding 50% (e.g., configurations 1-3, 1-4, and especially in 2-3)—highlighting its weaker performance.

The results suggest that the 'BPM DL' method is particularly effective across both used electrode systems (bipolar and tetrapolar). However, it also demonstrates an advantage of bipolar setups, where signal quality is typically lower. In bipolar configurations, which are generally more challenging due to higher noise and less optimal signal capture, 'BPM DL' still achieves lower MAPE values, indicating more accurate HR estimation compared to 'findpeaks'. The fact that 'BPM DL' performs well even in these difficult conditions highlights its robustness.

5. Discussion

During the presented research, we acquired the EBI signals using the selected electrode placements in perpendicular and distal placements relative to the wrist. Firstly, we analyzed the acquired signals concerning the modulation depth caused by the cardiac activity.

The measurement results demonstrate the significance of the electrode positioning relative to the arteries in the forearm. As can be seen from Table 2, distal placement provides a generally higher value of $\Delta Z(t)$. Irrespective of the electrode width, the highest values of $\Delta Z(t)$ are gained by using configuration B of both electrode widths—the longest distance between the electrodes. The same phenomenon appears also in perpendicular placement. Therefore, a longer distance between the electrodes is preferred in wearable device design, clearly related to the artery's locations. In the cases of such a wide gap between the electrodes as represented by the configurations B-b10 and B-b17 (Table 1), we expect the contribution from both arteries: radial and ulnar.

While the tetrapolar system provides the lowest result in terms of $\Delta Z(t)$, it provides remarkably higher S (sensitivity)—as seen in Figure 9. The bipolar system delivers higher values of $\Delta Z(t)$, while the signal is weaker and more interfered with noise (Figure 9). The tetrapolar system is practical when targeting arteries can be implemented, as reported in the literature before [15]. Such knowledge is important for algorithm development—a reasonable electrode configuration choice enables accurate HR estimation.

Secondly, the acquired signals underwent complex processing with the goal of adopting techniques and algorithms for HR estimation from the EBI signals.

In Figure 10, the left plot demonstrates the performance of the 'findpeaks' method when applying BPF and Savitzky–Golay filters. The scatter of points across the SNR and BPM difference ranges is noticeable, indicating variability in performance. Notably, the BPM consistently achieves higher SNR values, distributed more centrally and towards the upper third of the plot. To better analyze the scatter plot, the centroid of both data clusters was added as a diamond symbol with the same color as the corresponding data clusters. As can be observed from the centroid locations, the BPM achieves the highest SNR values and lowest BPM differences in the 'findpeaks' method's case, leaving the Savitzky–Golay processing method behind with 10 points of BPM differences, as well as with an approximately 1 dB lower SNR result for the relevant dataset.

In Figure 10, the right plot illustrates the 'BPM DL' method's performance under the same filtering conditions. Here, both results from filtered data show a pronounced clustering of points in the lower BPM difference region. Similar to 'findpeaks' scatter plot,

the BPM calculation indicates better performance in terms of SNR and $DIFF_{BPM}$ than the Savitzky–Golay filtering method. In this case, the difference between these two methods is much closer compared to $DIFF_{BPM}$ and SNR values.

In summary, across both plots, the BPF filter exhibits higher SNR values, suggesting effective noise management as well as in the BPM difference case. Since the signal is more smoothed compared to the one obtained with the Savitzky–Golay filter, see Figure 6, BPM estimation algorithms are less likely to detect any false peaks. The 'BPM DL' method outperforms 'findpeaks' in terms of noise robustness and BPM accuracy, particularly evident in its ability to cluster data points at lower BPM differences across a broad range of SNRs. This analysis underscores the critical impact of choosing appropriate filtering techniques and processing algorithms on the accuracy and reliability of BPM measurements.

In evaluating the performance of 'findpeaks' and 'BPM DL' algorithms based on the presented colormap graphs and scatter plots, it is clear that 'BPM DL' demonstrates significantly better results. This combination yielded improved accuracy in terms of BPM differences.

'BPM DL' also outperforms 'findpeaks' concerning MAPE values. A visual inspection of the colormap tables reveals consistently lower MAPE values for 'BPM DL', as indicated by the increased presence of green cells. Notably, the bipolar electrode 2-3 configuration performs better with 'BPM DL' while 'findpeaks' produces significantly higher MAPE values in this configuration. Similar to the $DIFF_{BPM}$ analysis, the 'BPM DL' method exhibits a clear advantage, demonstrating superior performance across all test subjects and nearly all electrode configurations. Only a few outliers, represented in distinct red on the DIFF colormap, indicate instances where performance was suboptimal.

When evaluating the electrode configurations, the tetrapolar setup consistently demonstrates strong performance across all tables, as expected. However, certain bipolar configurations also yield promising results. For instance, electrode placements 1-3 and 1-4, when processed with the BPF method, show stable and reliable outcomes in both MAPE and $DIFF_{BPM}$ metrics, indicating potential advantages for these configurations. Conversely, electrode placement 2-3 exhibits significantly poorer performance, with noticeably higher MAPE and $DIFF_{BPM}$ values, as well as lower SNR—highlighting the drawbacks of this configuration in accurately capturing cardiac activity signals.

The developed algorithm estimates the BPM by identifying the best frequency that correlates with the EBI signal (using cross-correlation) and then detecting the signal peaks to determine the HR more accurately. Finally, it calculates BPM based on the time differences between the peak locations. The strengths of this approach are:

1. Frequency analysis: The methodology performs a comprehensive frequency analysis of the EBI signal by dividing it into segments, each analyzed for the best frequency component. This approach can capture variations in HR over time, making it suitable for applications where HR may change dynamically.
2. Robustness: The methodology uses cross-correlation to find the best frequency for each segment. This approach is robust to noise and can adapt to different signal characteristics, making it suitable for real-world scenarios.
3. Peak detection: The code incorporates peak detection to identify heartbeats in the EBI signal. This step further refines the BPM value estimation, making it suitable for precise timing applications.
4. Outlier handling: The code implements outlier detection and correction, ensuring that spurious BPM values are replaced with more reliable estimates, enhancing the accuracy and reliability of the final BPM values.

6. Conclusions

To summarize, this work presents a small-scale experimental study on electrode placement and number for recording bioimpedance signals at the wrist. The signals are processed with a custom signal processing pipeline and algorithm to: (1) detect signal quality using a custom SNR metric and (2) estimate the subject's heart rate (HR). The HR detection results are validated using PPG as the reference signal.

The main findings include:

- Confirmation that focusing on the signal source (i.e., the pulsating flow of arterial blood) offers benefits, demonstrating that it is feasible to use peripheral body sites, such as the wrist, for noninvasive and accurate HR acquisition. The distal placement provides higher $\Delta Z(t)$ (up to 0.231 Ω) when electrodes are positioned on both wrist arteries.
- Quantification of the advantages of the tetrapolar electrode setup, with further evidence that bipolar setups are also feasible. Generally, the bipolar system results in a larger $\Delta Z(t)$, while the tetrapolar setup provides greater sensitivity.
- Comparison of bandpass and Savitzky–Golay filters during the preprocessing stage. The bandpass filter consistently yields higher SNR metrics and lower BPM estimation errors, when used with either of the two HR estimation algorithms. Specifically, the bandpass filter achieves 3.6 dB average SNR for the best bipolar setup and 4.8 dB average SNR for the tetrapolar setup, while the Savitzky–Golay filter shows 2.6 and 3.3 dB SNR, respectively.
- Comparison of the custom HR estimation algorithm ('BPM DL') with the standard 'findpeaks' method as implemented in MATLAB. The 'BPM DL' algorithm shows a reduction in both relative and absolute HR estimation errors. Specifically, 'BPM DL' achieves an absolute error as low as 1.8 BPM (with 3.1 BPM STD) for the best bipolar setup and 2.4 BPM absolute error (with 4.3 BPM STD) for the best tetrapolar setup combined with the preprocessing algorithm. The respective values for the 'findpeaks' method are 17.2 BPM (7.2 BPM STD) and 6.2 BPM (7.1 BPM STD). The differences in relative errors are similar.
- Of the four combinations of filtering algorithms paired with HR estimation algorithms, the 'BPM DL' algorithm combined with the bandpass filter demonstrates the best results across a range of noisy signals.

Author Contributions: Conceptualization, D.L. and M.M.; methodology, D.L., M.M. and A.K.; validation, D.L. and M.M.; formal analysis, D.L., M.M. and A.K.; investigation, D.L. and M.M.; data curation, D.L.; writing—original draft preparation, D.L., M.M. and A.K.; writing—review and editing, D.L., M.M., R.J., O.M. and A.E.; visualization, D.L. and M.M.; supervision, O.M. and A.E.; project administration, D.L.; funding acquisition, O.M. and A.E. All authors have read and agreed to the published version of the manuscript.

Funding: This research was supported by the Estonian Research Council (Grant PRG1483) and in part by the European Union, Grant Agreement n. 101095672 (project PRAESIIDIUM "Physics informed machine learning-based prediction and reversion of impaired fasting glucose management").

Institutional Review Board Statement: The study was conducted in accordance with the Declaration of Helsinki, and approved by the Life and Medical Sciences Research Ethics Committee of the University of Latvia (protocol number 71-35/160, approval date: 10 November 2023) for studies involving humans.

Informed Consent Statement: Informed consent was obtained from all subjects involved in the study.

Data Availability Statement: The data presented in this study are available on request from the corresponding author. The data are not publicly available due to the ethical reasons as it contains sensitive personal data (cardiac information).

Conflicts of Interest: The authors declare no conflicts of interest.

Abbreviations

The following abbreviations are used in this manuscript:

BPM	Beats Per Minute
BPF	Band-pass Filter
EBI	Electrical Bioimpedance
ICG	Impedance Cardiography
IIR	Infinite Impulse Response
MAPE	Mean Absolute Percentage Error
HR	Heart Rate
PPG	Photoplethysmography
SNR	Signal-to-Noise Ratio

References

1. Li, K.; Cardoso, C.; Moctezuma-Ramirez, A.; Elgalad, A.; Perin, E. Heart Rate Variability Measurement through a Smart Wearable Device: Another Breakthrough for Personal Health Monitoring? *Int. J. Environ. Res. Public Health* **2023**, *20*, 7146. [CrossRef] [PubMed]
2. Draghici, A.E.; Taylor, J.A. The physiological basis and measurement of heart rate variability in humans. *J. Physiol. Anthropol.* **2016**, *35*, 22. [CrossRef] [PubMed]
3. Zaza, A.; Ronchi, C.; Malfatto, G. Arrhythmias and Heart Rate: Mechanisms and Significance of a Relationship. *Arrhythmia Electrophysiol. Rev.* **2018**, *7*, 232–237. [CrossRef]
4. De Pinho Ferreira, N.; Gehin, C.; Massot, B. A Review of Methods for Non-Invasive Heart Rate Measurement on Wrist. *IRBM* **2021**, *42*, 4–18. [CrossRef]
5. Naranjo-Hernández, D.; Reina-Tosina, J.; Min, M. Fundamentals, Recent Advances, and Future Challenges in Bioimpedance Devices for Healthcare Applications. *J. Sens.* **2019**, *2019*, 9210258. [CrossRef]
6. Martinsen, O.G.; Grimnes, S. *Bioimpedance and Bioelectricity Basics*, 3rd ed.; Academic Press: New York, NY, USA, 2014.
7. Patterson, R. Fundamentals of impedance cardiography. *IEEE Eng. Med. Biol. Mag.* **1989**, *8*, 35–38. [CrossRef]
8. Escalona, O.; Cullen, N.; Weli, I.; McCallan, N.; Ng, K.Y.; Finlay, D. Robust Arm Impedocardiography Signal Quality Enhancement Using Recursive Signal Averaging and Multi-Stage Wavelet Denoising Methods for Long-Term Cardiac Contractility Monitoring Armbands. *Sensors* **2023**, *23*, 5892. [CrossRef] [PubMed]
9. Metshein, M.; Gautier, A.; Larras, B.; Frappe, A.; John, D.; Cardiff, B.; Annus, P.; Land, R.; Martens, O. Study of Electrode Locations for Joint Acquisition of Impedance- and Electro-cardiography Signals. In Proceedings of the 2021 43rd Annual International Conference of the IEEE Engineering in Medicine & Biology Society (EMBC), Guadalajara, Mexico, 1–5 November 2021; p. 7264. [CrossRef]
10. Mejía-Mejía, E.; May, J.M.; Torres, R.; Kyriacou, P.A. Pulse rate variability in cardiovascular health: A review on its applications and relationship with heart rate variability. *Physiol. Meas.* **2020**, *41*, 07TR01. [CrossRef]
11. Landaeta, R.G.; Casas, O.; Pallas-Areny, R. Heart Rate Detection from Plantar Bioimpedance Measurements. In Proceedings of the 2006 International Conference of the IEEE Engineering in Medicine and Biology Society, New York, NY, USA, 30 August–3 September 2006; pp. 5113–5116. [CrossRef]
12. Periyasamy, V.; Pramanik, M.; Ghosh, P.K. Review on heart-rate estimation from photoplethysmography and accelerometer signals during physical exercise. *J. Indian Inst. Sci.* **2017**, *97*, 313–324. [CrossRef]
13. Sel, K.; Osman, D.; Huerta, N.; Edgar, A.; Pettigrew, R.I.; Jafari, R. Continuous cuffless blood pressure monitoring with a wearable ring bioimpedance device. *npj Digit. Med.* **2023**, *6*, 59. [CrossRef]
14. Kassanos, P. Bioimpedance Sensors: A Tutorial. *IEEE Sens. J.* **2021**, *21*, 22190–22219. [CrossRef]
15. Metshein, M.; Pesti, K.; Lapsa, D.; Annus, P.; Janeliukstis, R.; Elsts, A.; Martens, O. Evaluation of Two-Electrode System Configurations for Forearm Arteries Bioimpedance Measurement. In Proceedings of the 2024 IEEE International Instrumentation and Measurement Technology Conference (I2MTC), Glasgow, UK, 20–23 May 2024; pp. 1–6. [CrossRef]
16. Yılmaz, K.; Adeyemi, A.; Antink, C.H.; Vehkaoja, A. Comparison of Electrode Configurations for Impedance Plethysmography Based Heart Rate Estimation at the Forearm. In Proceedings of the 2022 IEEE Sensors, Dallas, TX, USA, 30 October–2 November 2022; pp. 1–4. [CrossRef]
17. Lapsa, D.; Janeliukštis, R.; Elsts, A. Electrode Comparison for Heart Rate Detection via Bioimpedance Measurements. In Proceedings of the 2022 Workshop on Microwave Theory and Techniques in Wireless Communications (MTTW), Riga, Latvia, 5–7 October 2022; pp. 41–46. [CrossRef]
18. Priidel, E.; Annus, P.; Metshein, M.; Land, R.; Märtens, O.; Min, M. Lock-in integration for detection of tiny bioimpedance variations. In Proceedings of the 2018 16th Biennial Baltic Electronics Conference (BEC), Tallinn, Estonia, 8–10 October 2018; pp. 1–4. [CrossRef]
19. Jung, M.H.; Namkoong, K.; Lee, Y.; Jun Koh, Y.; Eom, K.; Jang, H.; Jung, W.; Bae, J.; Park, J. Wrist-wearable bioelectrical impedance analyzer with miniature electrodes for daily obesity management. *Sci. Rep.* **2021**, *11*, 1238. [CrossRef] [PubMed]

20. Kekonen, A.; Bergelin, M.; Johansson, M.; Kumar Joon, N.; Bobacka, J.; Viik, J. Bioimpedance sensor array for long-term monitoring of wound healing from beneath the primary dressings and controlled formation of H2O2 using low-intensity direct current. *Sensors* **2019**, *19*, 2505. [CrossRef]
21. Alsanie, S.; Lim, S.; Wootton, S. Detecting low-intake dehydration using bioelectrical impedance analysis in older adults in acute care settings: A systematic review. *BMC Geriatr.* **2022**, *22*, 954. [CrossRef]
22. Hoog Antink, C.; Schulz, F.; Leonhardt, S.; Walter, M. Motion Artifact Quantification and Sensor Fusion for Unobtrusive Health Monitoring. *Sensors* **2018**, *18*, 38. [CrossRef]
23. Lapsa, D.; Janeliukstis, R.; Elsts, A. Adaptive Signal-to-Noise Ratio Indicator for Wearable Bioimpedance Monitoring. *Sensors* **2023**, *23*, 8532. [CrossRef]
24. Cömert, A.; Hyttinen, J. Investigating the possible effect of electrode support structure on motion artifact in wearable bioelectric signal monitoring. *Biomed. Eng. OnLine* **2015**, *14*, 44. [CrossRef]
25. Kusche, R.; Ryschka, M. Combining Bioimpedance and EMG Measurements for Reliable Muscle Contraction Detection. *IEEE Sens. J.* **2019**, *19*, 11687–11696. [CrossRef]
26. Cömert, A.; Honkala, M.; Hyttinen, J. Effect of pressure and padding on motion artifact of textile electrodes. *Biomed. Eng. OnLine* **2013**, *12*, 26. [CrossRef]
27. Dang, T.H.; Jang, G.Y.; Lee, K.; Oh, T.I. Motion Artifacts Reduction for Noninvasive Hemodynamic Monitoring of Conscious Patients Using Electrical Impedance Tomography: A Preliminary Study. *Sensors* **2023**, *23*, 5308. [CrossRef]
28. Metshein, M.; Abdullayev, A.; Gautier, A.; Larras, B.; Frappe, A.; Cardiff, B.; Annus, P.; Land, R.; Märtens, O. Sensor-Location-Specific Joint Acquisition of Peripheral Artery Bioimpedance and Photoplethysmogram for Wearable Applications. *Sensors* **2023**, *23*, 7111. [CrossRef] [PubMed]
29. Sel, K.; Osman, D.; Jafari, R. Non-Invasive Cardiac and Respiratory Activity Assessment From Various Human Body Locations Using Bioimpedance. *IEEE Open J. Eng. Med. Biol.* **2021**, *2*, 210–217. [CrossRef] [PubMed]
30. Wang, T.W.; Chu, H.W.; Chou, L.; Sung, Y.L.; Shih, Y.T.; Hsu, P.C.; Cheng, H.M.; Lin, S.F. Bio-Impedance Measurement Optimization for High-Resolution Carotid Pulse Sensing. *Sensors* **2021**, *21*, 1600. [CrossRef]
31. Ren, B.; Wang, Z.; Ma, K.; Zhou, Y.; Liu, M. An Improved Method of Heart Rate Extraction Algorithm Based on Photoplethysmography for Sports Bracelet. *Information* **2023**, *14*, 297. [CrossRef]
32. Kromka, J.; Saliga, J.; Kovac, O.; De Vito, L.; Picariello, F.; Tudosa, I. Radial artery pulse wave estimation by compressed sensing measurements of wrist bio-impedance. *Measurement* **2023**, *219*, 113174. [CrossRef]
33. Krivošei, A.; Min, M.; Annus, P.; Märtens, O.; Metshein, M.; Lotamõis, K.; Rist, M. Hankel Matrix Based Algorithm for Cardiac Pulse Wave Base and Peak Lines Correction. In Proceedings of the 2022 IEEE International Symposium on Medical Measurements and Applications (MeMeA), Messina, Italy, 22–24 June 2022; pp. 1–6. [CrossRef]
34. Wójcikowski, M.; Pankiewicz, B. Photoplethysmographic Time-Domain Heart Rate Measurement Algorithm for Resource-Constrained Wearable Devices and its Implementation. *Sensors* **2020**, *20*, 1783. [CrossRef]
35. Han, J.; Ou, W.; Xiong, J.; Feng, S. Remote Heart Rate Estimation by Pulse Signal Reconstruction Based on Structural Sparse Representation. *Electronics* **2022**, *11*, 3738. [CrossRef]
36. He, Z. The control mechanisms of heart rate dynamics in a new heart rate nonlinear time series model. *Sci. Rep.* **2020**, *10*, 4814. [CrossRef] [PubMed]
37. Alharbi, Y.; Alshrouf, A.; Mansouri, S. Heart Rate Monitoring Using Electrical Impedance. In Proceedings of the 2021 Seventh International conference on Bio Signals, Images, and Instrumentation (ICBSII), Chennai, India, 25–27 March 2021; pp. 1–4. [CrossRef]
38. Zurich Instruments. *MFIA User Manual*; Zurich Instruments: Zurich, Switzerland, 2023.
39. Aliau-Bonet, C.; Pallas-Areny, R. A Novel Method to Estimate Body Capacitance to Ground at Mid Frequencies. *IEEE Trans. Instrum. Meas.* **2013**, *62*, 2519–2525. [CrossRef]
40. Matlab Filter Design. Available online: https://se.mathworks.com/help/signal/ref/filtfilt.html (accessed on 11 August 2024).
41. Lee, J.; Kim, S.; Lee, D. Fast cross-correlation method for real time detection of fetal heart rate. In Proceedings of the 20th Annual International Conference of the IEEE Engineering in Medicine and Biology Society. Vol. 20 Biomedical Engineering Towards the Year 2000 and Beyond (Cat. No.98CH36286), Hong Kong, China, 1 November 1998; Volume 20, pp. 178–181. [CrossRef]
42. Horvatic, D.; Stanley, H.E.; Podobnik, B. Detrended cross-correlation analysis for non-stationary time series with periodic trends. *Europhys. Lett.* **2011**, *94*, 18007. [CrossRef]

Disclaimer/Publisher's Note: The statements, opinions and data contained in all publications are solely those of the individual author(s) and contributor(s) and not of MDPI and/or the editor(s). MDPI and/or the editor(s) disclaim responsibility for any injury to people or property resulting from any ideas, methods, instructions or products referred to in the content.